Molecular Crystals and Liquid Crystals
Publication details, including instructions for authors and subscription information:
http://www.tandfonline.com/loi/gmcl20

Simulating the Emission Properties of Luminescent Dyes within One-Dimensional Uniaxial Liquid Crystal Microcavities

Lieven Penninck [a], Patrick De Visschere [a], Jeroen Beeckman [a] & Kristiaan Neyts [a]
[a] Ghent University, Electronics and Information Systems Department, Ghent, Belgium

Version of record first published: 15 May 2012.

To cite this article: Lieven Penninck , Patrick De Visschere , Jeroen Beeckman & Kristiaan Neyts (2012): Simulating the Emission Properties of Luminescent Dyes within One-Dimensional Uniaxial Liquid Crystal Microcavities, Molecular Crystals and Liquid Crystals, 560:1, 82-92

To link to this article: http://dx.doi.org/10.1080/15421406.2012.663181

Mol. Cryst. Liq. Cryst., Vol. 560: pp. 82–92, 2012

ISSN: 1542-1406 print/1563-5287 online
DOI: 10.1080/15421406.2012.663181

Taylor & Francis
Taylor & Francis Group

Simulating the Emission Properties of Luminescent Dyes within One-Dimensional Uniaxial Liquid Crystal Microcavities

LIEVEN PENNINCK,* PATRICK DE VISSCHERE, JEROEN BEECKMAN, AND KRISTIAAN NEYTS

Ghent University Electronics and Information Systems Department, Ghent, Belgium

We have developed a simulation method which is capable of simulating the emissive properties of luminescent dyes inside uniaxial anistropic thin film microcavities[1]. The method uses plane wave decomposition of the electric field of a dipole antenna in a uniaxial medium and a scattering matrix formalism to account for interference and reflection from the various interfaces in the device. We apply this method to simulate the excitation of waveguide modes in a slab waveguide formed by reorientation of a liquid crystal. We investigate the emission both outside the device and into waveguided modes inside the liquid crystal device.

Keywords Plane waves; waveguides; thin films; fluorescence; liquid crystals

1. Introduction

In recent years many liquid crystal based optical devices have been reported outside of their use in displays, such as: liquid crystal lasers [2], luminescent solar concentrators [3], tunable waveguide devices [4], switchable/tunable filters [5], organic LEDs [6], single photon sources with definite polarizations [7] ... Many other applications have been demonstrated or suggested, a more complete overview can be found in a review paper [8].

With the growing number and increasing diversity of applications for liquid crystals, there is a need for accurate simulation and design tools for such applications. In this article we present a simulation method to calculate the radiation of an electrical dipole antenna inside a thin anisotropic film or in a stack of uniaxially anisotropic layers and apply it to the case of an emitting dye inside a liquid crystal cell with varying director profile.

Our method is based upon the decomposition of the dipole field into a superposition of plane and evanescent waves. The radiation pattern of the dipole inside the layer structure is modified by reflection, transmission and interferences of these waves by interfaces inside the layer stack. Simulation of one-dimensional thin film stacks using plane wave decomposition was pioneered by Lukosz [9] and has been applied in many fields [10] for stacks containing only isotropic materials. The method we present here can simulate the radiation of an electric dipole antenna inside a stack of one-dimensional anisotropic layers with arbitrary orientation of the optical axes. Earlier methods are restricted to stacks of

*Address correspondence to Liven Penninck, ELIS Department, Ghent University, St. Pieters nieuwstraat 41, 9000 Gent, Belgium. E-mail: lieven.penninck@elis.ugent.be

isotropic materials or to stacks of uniaxial anisotropic materials with specific orientations of the optic axis [11]. Other methods such as the finite-difference-time-domain (FDTD) method or rigorous coupled wave analysis (RCWA) can be used to model the radiation from non-planar structures at the expense of more computation resources [12, 13].

In section 2 the plane wave decomposition of the dipole field in an infinite medium and the alterations of the dipole field caused by layered stacks are described. In section 3 the method is applied to simulate the emission properties of a fluorescent dye inside a liquid crystal waveguide formed by reorientation of the director. We summarize our results in section 4.

2. Plane Wave Simulation Method for Anisotropic Thin Film Devices

2.1 Physical Background & Notations

We consider the problem of a radiating elementary electrical dipole inside a stack of uniaxial anisotropic one-dimensional layers. The problem of a classical elementary electrical dipole antenna is equivalent to the emission of photons by an ensemble of excited states decaying through an electric dipole transition [14]. The coordinate system is chosen so that the x- and y-axis are parallel to the layer stack and the z-axis is normal to the stack. The orientation of the dipole moment $\mathbf{p}$ is defined by an inclination angle ν (with respect to the z-axis) and an azimuth angle ζ in the xy-plane. We choose the origin of the xyz-system to coincide with the location of the dipole. Each uniaxial medium i inside the layer stack is characterized by the orientation of the optical axis $\mathbf{c}_\mathrm{i}$ (extra-ordinary polarization) and the two eigenvalues of the dielectric tensor $\varepsilon_\perp$ and $\varepsilon_\parallel$, where $\varepsilon_\perp$ and $\varepsilon_\parallel$ are the eigenvalues respectively in a plane perpendicular (ordinary polarization) and parallel to $\mathbf{c}_\mathrm{i}$. The orientation of $\mathbf{c}_\mathrm{i}$ is also determined by an inclination angle α_i and azimuth angleβ_i. A sketch of the coordinate system and layer stack is presented in Fig. 1.

Any monochromatic electric field $\mathbf{E}$ can be written as a superposition of plane and evanescent waves. The electric field of a single plane or evanescent wave is written as:

$$\mathbf{E} = \mathbf{E}_0 exp(j\omega t - jk_x x - jk_y y \mp jk_z z) \tag{1}$$

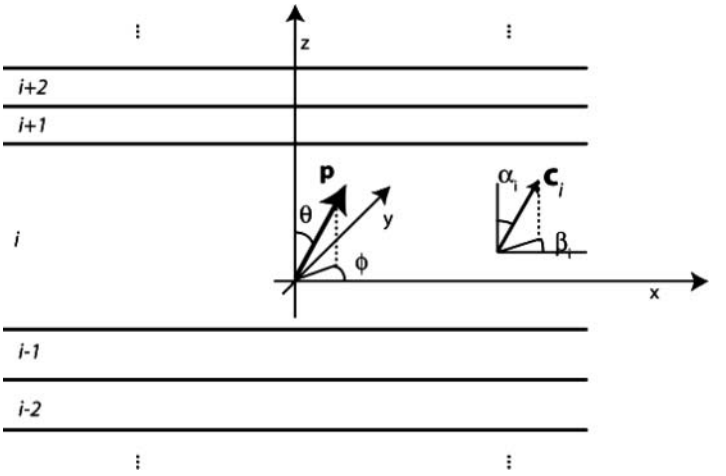

Figure 1. Coordinate system and definition of inclination and azimuth angles.

and there is a similar expression for the magnetic field **H**. ω is the angular frequency of the dipole antenna. Each plane or evanescent wave is characterized by its wave-vector **k**:

$$\mathbf{k} = \begin{pmatrix} k_x \\ k_y \\ k_z \end{pmatrix} = \kappa \mathbf{1}_\kappa + k_z \mathbf{1}_z = k_\perp \mathbf{1}_\perp + k_\parallel \mathbf{1}_c \tag{2}$$

Because of Snell's law waves with given k_x and k_y only couple to waves with the same k_x and k_y in the other media. This transverse part of **k** can be grouped to $\kappa = (k_x^2 + k_y^2)^{1/2}$. In an anisotropic medium the value for k_z depends on the medium and the polarization of the plane wave. The wave-vector can also be written as a sum of a part perpendicular $\mathbf{k}_\perp$ and a part parallel $k_\parallel$ to **c**. The amplitude of the wave-vector in medium i is given by $k_i = 2\pi n_{i,e/o}/\lambda$ the z-component can be found with $k_{z,i/e} = \sqrt{k_i^2 - \kappa^2}$. λ is the wavelength of the light in vacuum and n_i is the refractive index. For uniaxial anisotropic media there is a different refractive index for the ordinary waves $n_{i,o}$ and extra ordinary waves $n_{i,e}$. The value of $n_{i,o}$ is the same for every direction in the medium but $n_{i,e}$ depends on the direction of propagation. Throughout this paper the subscripts$\parallel$, $\perp$and z are used to denote components respectively parallel to **c**, perpendicular to **c** and parallel to z.

A plane wave with $\kappa < k_i$ travels in a certain direction, the inclination angle of propagation is found with $sin(\theta) = \kappa/k_{i,e/o}$, the azimuth angle is found with $tan(\phi) = k_y/k_x$. When $\kappa > k_i$, k_z is an imaginary number and the wave is an evanescent wave that decays exponentially with z. In non-absorbing media no power is dissipated by evanescent waves. No direction of propagation can be associated with evanescent waves since these only have a non-zero field in a small area. Evanescent waves represent the near-field of the dipole.

2.2 Radiation of Elementary Dipoles in a Homogeneous Anisotropic Medium

The starting point of our simulation is the plane wave expansion of the electric field of a dipole antenna in an infinite anisotropic medium [1]. The following expressions are found for the ordinary and extra-ordinary polarized wave (for $z > 0$):

$$\mathbf{E}_o = \frac{-j}{8\pi^2} \int_{-\infty}^{+\infty}\int_{-\infty}^{+\infty} dk_x dk_y \left[\mathbf{k}_\perp \times \frac{\mu\omega^2}{k_\perp^2} \frac{\mathbf{c}\cdot(\mathbf{k}_\perp \times \mathbf{p}_\perp)}{k_{z,o,+}}\mathbf{c}\right] \exp[-j(k_x x + k_y y + k_{z,o,+} z)] \tag{3}$$

$$\mathbf{E}_e = \frac{-j}{8\pi^2} \int_{-\infty}^{+\infty}\int_{-\infty}^{+\infty} dk_x dk_y \left(\frac{k_\parallel p_\parallel}{\varepsilon_\parallel} - \frac{k_\parallel^2 (\mathbf{k}_\perp \cdot \mathbf{p}_\perp)}{k_\perp^2 \varepsilon_\perp}\right) \frac{\mathbf{k}_\perp - \frac{k_\perp^2 \varepsilon_\perp}{k_\parallel^2 \varepsilon_\parallel}\mathbf{k}_\parallel}{\frac{\varepsilon_\perp + \Delta\varepsilon c_z^2}{\varepsilon_\parallel}\left(k_{z,e,+} + \frac{\Delta\varepsilon c_t c_z \kappa}{\varepsilon_\perp + \Delta\varepsilon c_z^2}\right)}$$
$$\times \exp[-j(k_x x + k_y y + k_{z,e,+} z)] \tag{4}$$

and a similar expression for $z<0$. The field is decomposed in plane wave eigenmodes which can be readily used in multilayer stack algorithms, as explained in section 2.3. Another approach is to start from the formulas for the radiation of a dipole in vacuum and to anisotropically transform the problem using the method of Clemmow [15]. The results from both approaches are in agreement. For the field in (3), $k_{z,o,\pm}$ is independent of the direction of **c**, this is called the ordinary polarization. For the field in (4), $k_{z,e,\pm}$ does depend on the direction of **c** and $\mathbf{E}_e$ is called the extra-ordinary polarization. From the expression of **E**, **H** can be determined using $-j\mathbf{k} \times \mathbf{E_{e/o}} = -j\omega\mu\mathbf{H_{e/o}}$, bearing in mind that the value of k_z depends on the polarization.

The power flux through a plane with constant z radiated by a dipole is then found by integrating the z-component of the Poynting vector $\mathbf{S}$ (unit W/m^2) over that plane:

$$\mathbf{S}_z = \frac{1}{2}\mathrm{Re}[\mathbf{E} \times \mathbf{H}^*]_z \tag{5}$$

The * denotes complex conjugation. $\mathbf{E}$ and $\mathbf{H}$ in Eq. (5) are two separate double integrals over $\mathrm{d}k_x\ \mathrm{d}k_y$. When integrating over a plane of constant z we can bring both $\mathbf{E}$ and $\mathbf{H}$ under the same double integral. Because of orthogonality an extra factor $4\pi^2$ is needed in the new integrand K:

$$\begin{aligned}\int_{-\infty}^{+\infty}\int_{-\infty}^{+\infty} \mathbf{S}_z dx dy &= \int_{-\infty}^{+\infty}\int_{-\infty}^{+\infty} 2\pi^2 Re[\mathbf{E}(k_x, k_y) \times \mathbf{H}(k_x, k_y)^*]_z dk_x dk_y \\ &= \int_{-\infty}^{+\infty}\int_{-\infty}^{+\infty} K(k_x, k_y) dk_x dk_y \end{aligned} \tag{6}$$

The integrand K (unit W.m^2) can be split in an ordinary K_o and an extra ordinary part K_e. K is calculated for the field in a plane with $z > 0$ (K^+) or a plane with $z < 0$ (K^-). The total power radiated by a dipole F (in W) is:

$$F = \int_{-\infty}^{+\infty}\int_{-\infty}^{+\infty} [K_o^+ + K_e^+ + K_o^- + K_e^-] dk_x dk_y \tag{7}$$

From Eq. (3) and (4) it is also possible to derive the unit vectors of the ordinary and extra-ordinary eigenmodes of a uniaxial medium. The electric field of a mode is found by multiplying the unit vector with a complex amplitude. Looking at Eq. (8) and (9) it is clear that the ordinary field cannot have a component along $\mathbf{c}$ but the extra-ordinary field can.

$$\mathbf{1_o} = \frac{\mathbf{k} \times \mathbf{c}}{|\mathbf{k} \times \mathbf{c}|} \tag{8}$$

$$\mathbf{1_e} = \frac{\mathbf{k}_\perp - \frac{\mathbf{k}_\perp^2 \varepsilon_\perp}{\mathbf{k}_\parallel \varepsilon_\parallel}\mathbf{c}}{\left|\mathbf{k}_\perp - \frac{\mathbf{k}_\perp^2 \varepsilon_\perp}{\mathbf{k}_\parallel \varepsilon_\parallel}\mathbf{c}\right|} \tag{9}$$

2.3 Radiation of a Dipole Inside an Anisotropic Microcavity

The radiation pattern of a dipole antenna can be significantly altered by placing the dipole inside an optical microcavity [16]. Interferences between reflections at the different layer interfaces cause variations in the local density of states at the location of the dipole antenna. As a result the angular emission pattern of the dipole is modified, this is also called the Purcell effect. The lateral dimensions of the films are much larger than their thicknesses and so the microcavities are in good approximation one-dimensional.

For an anisotropic microcavity a similar method can be applied to calculate the radiation of a dipole in the cavity. The eigenmodes of anisotropic materials are two linearly polarized waves, the ordinary (o) and the extraordinary (e) wave. The normalized fields of the eigenmodes are given by Eq. (8) and (9). The complex amplitude $E^+_{\infty,e/o}$ of each mode in

an infinite medium is given by Eq. (3) and(4). The amplitude $E^{-}_{\infty,e/o}$of modes travelling in the $-z$ direction is found with the corresponding expression for $z < 0$. The polarization state of the light is determined by the complex amplitudes of the ordinary and extra-ordinary waves and their difference in phase. One must be careful to simulate all changes in polarization that occur during propagation and reflection or transmission in an anisotropic cavity. In anisotropic media e- and o-waves are coupled when reflection or transmission at an interface takes place and reflection matrices,which describe the coupling between the two polarizations, should be used.

$$\begin{bmatrix} E^{+}_{Cav,o} \\ E^{+}_{Cav,e} \end{bmatrix} = \left(1 - \overline{\overline{A^{-}}}\,\overline{\overline{A^{+}}}\right)^{-1} \left(\begin{bmatrix} E^{+}_{\infty,o} \\ E^{+}_{\infty,e} \end{bmatrix} + \overline{\overline{A^{-}}} \begin{bmatrix} E^{-}_{\infty,o} \\ E^{-}_{\infty,e} \end{bmatrix} \right) \tag{10}$$

$$\begin{bmatrix} E^{-}_{Cav,o} \\ E^{-}_{Cav,e} \end{bmatrix} = \left(1 - \overline{\overline{A^{+}}}\,\overline{\overline{A^{-}}}\right)^{-1} \left(\begin{bmatrix} E^{-}_{\infty,o} \\ E^{-}_{\infty,e} \end{bmatrix} + \overline{\overline{A^{+}}} \begin{bmatrix} E^{+}_{\infty,o} \\ E^{+}_{\infty,e} \end{bmatrix} \right) \tag{11}$$

The reflection matrices $\overline{\overline{A^{\pm}}}$ are:

$$\overline{\overline{A^{\pm}}} = \begin{bmatrix} A^{\pm}_{oo} & A^{\pm}_{eo} \\ A^{\pm}_{oe} & A^{\pm}_{ee} \end{bmatrix} \tag{12}$$

where A_{lm} is the amplitude reflection coefficient for an incoming wave with polarization l into a reflected wave with polarization m, the reflection matrix takes into account both the reflection at the interfaces and phase changes by propagation through the materials. For isotropic layer stacks o- and e-waves are uncoupled ($A_{eo} = A_{oe} = 0$).

To calculate the reflection matrix we employ the scattering matrix method introduced by Ko [17]. Other methods, such as the Berreman 4×4 matrix method [18], can also be applied but we have chosen the scattering matrix method because it is numerically more stable when dealing with evanescent waves and total internal reflection.

The scattering matrix method calculates a 4×4 scattering matrix $\overline{\overline{S_{iN}}}$ that relates incoming waves in layer i traveling upward [$E_{o,i,+}$, $E_{e,i,+}$] and in the top layer N traveling downward [$E_{o,N,-}$, $E_{e,N,-}$] with the outgoing waves in the top layer traveling upward [$E_{o,N,+}$, $E_{e,N,+}$] and in the layer i traveling downward [$E_{o,i,-}$, $E_{e,i,-}$]. $\overline{\overline{S_{iN}}}$ is a block matrix of four 2×2 matrices. A sketch of the input and output waves in the scattering matrix method is shown in Fig. 2.

$$\begin{pmatrix} E_{o,N,+} \\ E_{e,N,+} \\ E_{o,i,-} \\ E_{e,i,-} \end{pmatrix} = \begin{bmatrix} \overline{\overline{S_{iN,11}}} & \overline{\overline{S_{iN,12}}} \\ \overline{\overline{S_{iN,21}}} & \overline{\overline{S_{iN,22}}} \end{bmatrix} \begin{pmatrix} E_{o,i,+} \\ E_{e,i,+} \\ E_{o,N,-} \\ E_{e,N,-} \end{pmatrix} \tag{13}$$

Once the matrix $\overline{\overline{S_{iN}}}$ is determined, the reflection matrix $\overline{\overline{A^{+}}}$ and the transmission matrix $\overline{\overline{T^{+}}}$ can be identified. $\overline{\overline{A^{+}}}$ and $\overline{\overline{T^{+}}}$ link the outgoing waves to $E_{o,i,+}$ and $E_{e,i,+}$.

$$\overline{\overline{T^{+}}} = \overline{\overline{S_{iN,11}}}; \quad \overline{\overline{A^{+}}} = \overline{\overline{S_{iN,21}}} \tag{14}$$

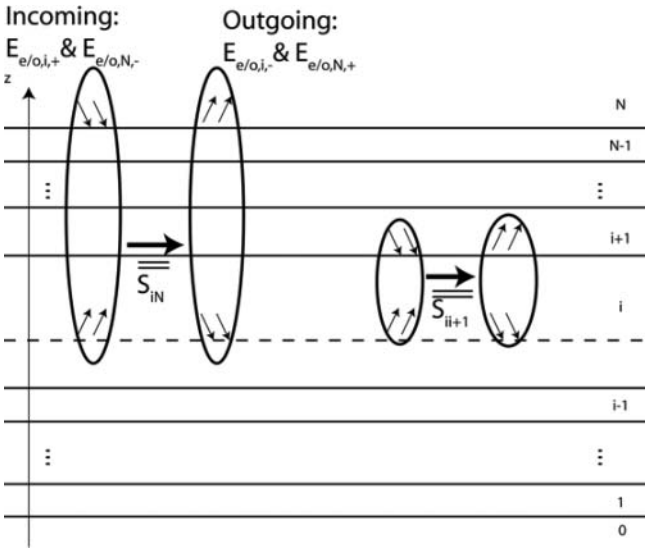

Figure 2. Sketch of the input-output relation of the scattering matrices. $\overline{\overline{S_{iN}}}$ is constructed by step by step addition of layers to $\overline{\overline{S_{ii}}}$.

An analogous procedure is used to determine $\overline{\overline{A^-}}$ and $\overline{\overline{T^-}}$. The fields emitted to the outside layer (N or 0) $\mathbf{E}_{out}$ can be calculated from $\mathbf{E}_{Cav}$:

$$\begin{bmatrix} E^{\pm}_{out,o} \\ E^{\pm}_{out,e} \end{bmatrix} = \overline{\overline{T^{\pm}}} \begin{bmatrix} E^{\pm}_{Cav,o} \\ E^{\pm}_{Cav,e} \end{bmatrix} \tag{15}$$

Starting from $\mathbf{E}_{out}$ the corresponding magnetic field $\mathbf{H_{out}}(-j\mathbf{k} \times \mathbf{E_{e/o}} = -j\omega\mu\mathbf{H_{e/o}})$ and Poynting vector (Eq. (5)) is calculated.

The scattering matrix of an entire stack $\overline{\overline{S_{iN}}}$ can be built by starting from $\overline{\overline{S_{ii}}}$ which is equal to the unity matrix and then adding extra layers step by step. Ko provides a formula for calculating the scattering matrix $\overline{\overline{S_{ij+1}}}$ of a stack with an additional layer when $\overline{\overline{S_{ij}}}$ and the matrix $\overline{\overline{I_j}}$ are known [17]. $\overline{\overline{I_j}}$ relates the fields above the *j+1/j* interface to the fields above the interface *j/j-1*.

$$\begin{pmatrix} E_{o,j+1,+} \\ E_{e,j+1,+} \\ E_{o,j+1,-} \\ E_{e,j+1,-} \end{pmatrix} = \overline{\overline{I_j}} \begin{pmatrix} E_{o,j,+} \\ E_{e,j,+} \\ E_{o,j,-} \\ E_{e,j,-} \end{pmatrix} \tag{16}$$

The relation between $\overline{\overline{S_{ij}}}$ and $\overline{\overline{S_{ij+1}}}$ is:

$$\overline{\overline{S_{ij+1,11}}} = \left(\overline{\overline{I_j}}^{-1}_{11} - \overline{\overline{S_{ij,12}}}\,\overline{\overline{I_j}}^{-1}_{21}\right)^{-1} \overline{\overline{S_{i,j,11}}} \tag{17}$$

$$\overline{\overline{S_{ij+1,12}}} = \left(\overline{\overline{I_j}}^{-1}_{11} - \overline{\overline{S_{ij,12}}}\,\overline{\overline{I_j}}^{-1}_{21}\right)^{-1} \left(\overline{\overline{S_{i,j,12}}}\,\overline{\overline{I_{j,22}}}^{-1} - \overline{\overline{I_j}}^{-1}_{12}\right) \tag{18}$$

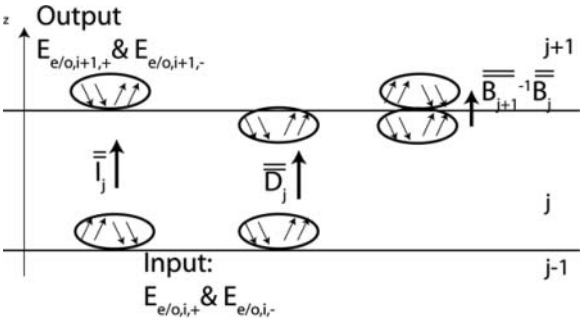

Figure 3. Sketch of the input and output waves of the matrix $\overline{\overline{I_j}}$. The phase propagation matrix $\overline{\overline{D_j}}$ and the matrices $\overline{\overline{B_j}}$ and $\overline{\overline{B_{j+1}}}$ relating the waves in medium j to the waves in medium j+1.

$$\overline{\overline{S_{ij+1,21}}} = \overline{\overline{S_{ij,22}}}\,\overline{\overline{I}}_{j\,21}^{-1}\,\overline{\overline{S_{ij+1,11}}} + \overline{\overline{S_{ij,21}}} \tag{19}$$

$$\overline{\overline{S_{ij+1,22}}} = \overline{\overline{S_{ij,22}}}\,\overline{\overline{I}}_{j\,21}^{-1}\,\overline{\overline{S_{ij+1,12}}} + \overline{\overline{S_{ij,22}}}\,\overline{\overline{I}}_{j\,22}^{-1} \tag{20}$$

We construct $\overline{\overline{I_j}}$ in the following way (a sketch is shown in figure 3). First the complex amplitudes of the input waves $[\mathrm{E}_{o,j,+}, \mathrm{E}_{e,j,+}, \mathrm{E}_{o,j,-}, \mathrm{E}_{e,j,-}]$ propagate from the *j-1/j* interface to the *j/j+1* interface, this causes a phase change proportional to the thickness of the layer d_j, expressed by the matrix $\overline{\overline{D_j}}$:

$$\overline{\overline{D_j}} = \exp\left(-jd_j\begin{bmatrix} k_{z,o,j,+} & 0 & 0 & 0 \\ 0 & k_{z,e,j,+} & 0 & 0 \\ 0 & 0 & k_{z,o,j,-} & 0 \\ 0 & 0 & 0 & k_{z,e,j,-} \end{bmatrix}\right) \tag{21}$$

At the interface *j/j+1* all transverse fields have to be constant, this is expressed by the following boundary conditions: $E_{x,j} = E_{x,j+1}$, $E_{y,j} = E_{y,j+1}$, $H_{x,j} = H_{x,j+1}$ and $H_{y,j} = H_{y,j+1}$. From the complex amplitudes of the four eigenmodes in medium *j+1* at the *j/j+1* interface and the unit fields of the four eigenmodes (given by Eq. (8) and (9)), the field components E_x, E_y, H_x and H_y at the *j/j+1* interface can be calculated. The matrix that links the amplitudes of the four eigenmodes in medium *j+1* with the four field components E_x, E_y, H_x and H_y at the *j/j+1* interface is written as $\overline{\overline{B_{j+1}}}$.

$$\begin{aligned}\begin{pmatrix} E_x \\ E_y \\ H_x \\ H_y \end{pmatrix} &= \begin{bmatrix} 1_{o,+,j+1,x} & 1_{e,+,j+1,x} & 1_{o,-,j+1,x} & 1_{e,-,j+1,x} \\ 1_{o,+,j+1,y} & 1_{e,+,j+1,y} & 1_{o,-,j+1,y} & 1_{e,-,j+1,y} \\ Y_{o,+,j+1,x} & Y_{e,+,j+1,x} & Y_{o,-,j+1,x} & Y_{e,-,j+1,x} \\ Y_{o,+,j+1,y} & Y_{e,+,j+1,y} & Y_{o,-,j+1,y} & Y_{e,-,j+1,y} \end{bmatrix}\begin{pmatrix} E_{o,j+1,+} \\ E_{e,j+1,+} \\ E_{o,j+1,-} \\ E_{e,j+1,-} \end{pmatrix} \\ &= \overline{\overline{B_{j+1}}}\begin{pmatrix} E_{o,j+1,+} \\ E_{e,j+1,+} \\ E_{o,j+1,-} \\ E_{e,j+1,-} \end{pmatrix}\end{aligned} \tag{22}$$

The matrix elements of the first two rows of $\overline{\overline{B_{j+1}}}$ are the *x*- and *y* components of Eq. (8) and (9). The corresponding magnetic field (per unit electric field) is found with

$\mathbf{Y_{e/o}} = \mathbf{k} \times \mathbf{1_{e/o}}/(\omega\mu)$ (unit $1/\Omega$), the x- and y-component are the respective matrix elements of the third and fourth row.

In summary (see figure 3), $\overline{\overline{D_j}}$ relates the amplitudes of the eigenmodes in medium j at the *j-1/j* interface to the amplitude of the eigenmodes in medium j at the *j+1/j* interface, $\overline{\overline{B_j}}$ (or $\overline{\overline{B_{j+1}}}$) relates the amplitudes of the four eigenmodes to the four transverse field components in medium j (or *j+1*) and $\overline{\overline{I_j}}$relates the amplitudes of the eigenmodes at the *j-1/j* interface in medium j to the amplitudes of the eigenmodes at the *j+1/j* interface in medium *j+1*. The boundary condition at the *j+1/j* interface can then be expressed as:

$$\overline{\overline{B_{j+1}}}\,\overline{\overline{I_j}} \begin{pmatrix} E_{o,j,+} \\ E_{e,j,+} \\ E_{o,j,-} \\ E_{e,j,-} \end{pmatrix} = \begin{pmatrix} E_{x,j+1} \\ E_{y,j+1} \\ H_{x,j+1} \\ H_{y,j+1} \end{pmatrix} = \begin{pmatrix} E_{x,j} \\ E_{y,j} \\ H_{x,j} \\ H_{y,j} \end{pmatrix} = \overline{\overline{B_j}}\,\overline{\overline{D_j}} \begin{pmatrix} E_{o,j,+} \\ E_{e,j,+} \\ E_{o,j,-} \\ E_{e,j,-} \end{pmatrix} \tag{23}$$

This equation has to hold for any input amplitudes [$E_{o,j,+}$, $E_{e,j,+}$, $E_{o,j,-}$, $E_{e,j,-}$], so that:

$$\overline{\overline{I_j}} = \overline{\overline{B_{j+1}}}^{-1}\overline{\overline{B_j}}\,\overline{\overline{D_j}} \tag{24}$$

With $\overline{\overline{B_j}}$, $\overline{\overline{B_{j+1}}}$ and $\overline{\overline{D_j}}$ given by Eq. (22) and (21), this equation allows to calculate $\overline{\overline{I_j}}$ for every layer. $\overline{\overline{S_{iN}}}$ is found with Eq. (17)-(20) after successively adding all layers. $\overline{\overline{T^+}}$ and $\overline{\overline{A^+}}$ are identified with Eq. (14).

3. Fluorescence in a Liquid Crystal Slab Waveguide

It is possible to create waveguides in liquid crystals by local reorientation of the liquid crystal molecules [19]. The variation can be made by thermal effects, optical reorientation or applying an electric field. The simulation method described above can be used to calculate the optical properties of waveguided modes inside slab waveguides in (or made of) liquid crystals. The structure is treated as a stack of discrete slabs. No limitation is imposed on the orientation of the liquid crystal inside the slabs. The advantage of this method is that it can simulate any kind of thin film optical structure with little computational effort.

As an example we calculate the radiation pattern of a fluorescent dye (the emission spectrum of 1% by weight of DCM in E7 was used) inside a one dimensional waveguide. First we compare the emission into waveguided modes and to the outside of the waveguide by different orientations of the transition dipole moment of the dye. Then we calculate the effective refractive index and the spectral excitation of each mode.

The configuration we used is sketched figure 4. A 5 μm thick layer of E7 is sandwiched between two optically thick glass substrates. For simplicity we assume the alignment layers have the same refractive as glass. The inclination angle of E7 is assumed to follow a Gaussian profile around the center (z = 0) of the LC layer. The profile of the inclination angle becomes $\alpha = 90^\circ - 90^\circ \exp(-z^2/2\sigma^2)$. The full width at half maximum of this profile is determined by σ ($FWHM = 2.355\sigma$), in this example we choose $\sigma = 500$ nm, $FWHM = 1178$ nm. The Gaussian profile is built up as a stack of homogeneous 50 nm thick layers with the inclination angle of each layer given by the Gaussian distribution for the middle of that layer. A small absorption term 0.0001j is added to the refractive indices of E7 $n_{e,E7}$ and $n_{o,E7}$ so that waveguided modes have a non-zero width.

A plot of the power emitted (K vs. κ/k_0) into plane waves propagating in the xz-plane is shown in figure 5 (for $\lambda = 606$ nm, the maximum of the dye spectrum). In the

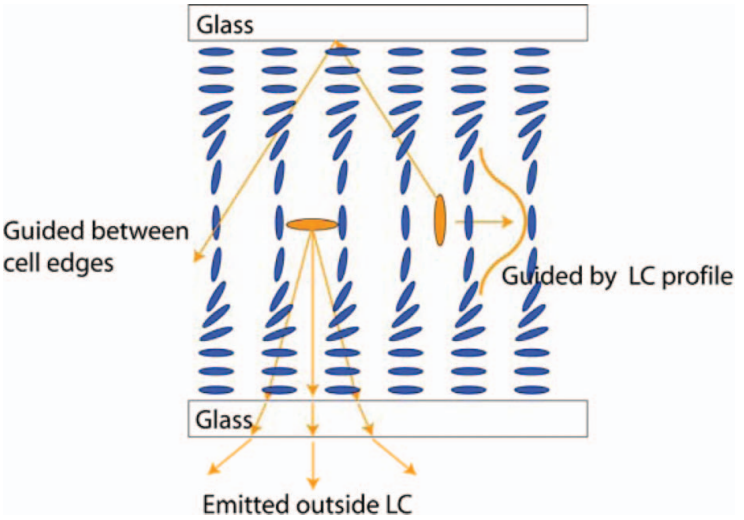

Figure 4. Sketch of the simulated configuration. A director profile in a planar aligned liquid crystal cell creates a waveguide for light emitted by fluorescent molecules inside the liquid crystal.

region $\kappa/k_0 = n_{glass}..n_{o,E7}$ waveguided modes occur for both o- and e-polarization. These are waves trapped in the entire LC-layer between the two glass substrates. For $\kappa/k_0 = n_{o,E7}..n_{e,E7}$ only e-polarized modes occur. These are waveguided by the refractive index profile created by the varying orientation of the LC inside the cell.

Dipole antennas (solid curve) that are parallel to the rubbing direction radiate partly to plane waves in the $\kappa/k_0 = 0...n_{glass}$ region. These plane waves are capable of escaping the liquid crystal cell and sometimes called "leaky modes". The other part is coupled to waveguided modes. Dipoles (dashed curve) which are oriented perpendicular to the rubbing (but still in plane with the substrate) only radiate to leaky modes. Perpendicular dipoles do not couple to waveguided modes because there is no overlap between the dipole electric field

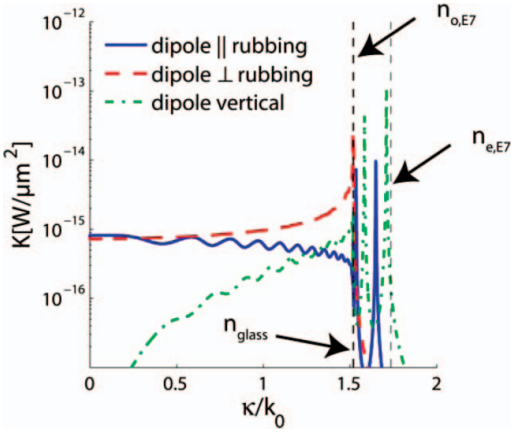

Figure 5. Power emitted K vs. in-plane wavevector κ/k_0 for different orientations of the transition dipole moment.

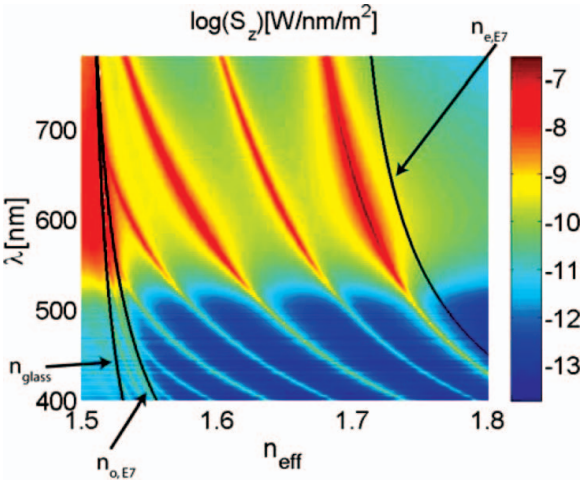

Figure 6. Spectral excitation of the waveguided modes by the laser dye DCM.

and the electric field of the waveguided modes. Dipoles in the z-direction (perpendicular to the substrate, dash-dotted curve) couple mainly to waveguided modes. It is interesting to note that dipoles along the z-direction couple to different modes than dipoles perpendicular to the rubbing. The z-dipoles couples to the even modes (0th and 2nd order), whereas the perpendicular dipole couples to odd modes (1st and 3d order). The effective refractive index $n_{eff} = \kappa/k_0$ of the 0th to 3d order mode is 1.7097, 1.6485, 1.5828 and 1.5342.

Figure 6 shows the coupling of an ensemble of randomly oriented dipoles (average over all three dipole directions) to the waveguided modes of the LC slab waveguide for the entire emission spectrum of the dye. This spectrum is simulated by weighing $K^+(k_x, k_y, \lambda)$ (radiation into individual plane) with the normalized emission spectrum $\int S_0(\lambda)d\lambda = 1$ of the dye in bulk E7. In Fig. 6 it is seen that n_{eff} increases with decreasing wavelength. As the wavelength decreases more modes are supported by the waveguide.

4. Conclusion

In this paper we presented a simulation method for light emission inside one dimensional liquid crystal devices. The electric field of an elementary dipole inside an anisotropic layer is written as a superposition of plane and evanescent waves. A scattering matrix formalism for plane and evanescent waves is used to calculate the emission inside one-dimensional microcavities. As an example we calculated the spectral excitation by a fluorescent dye of the waveguided modes of a liquid crystal slab waveguide. The coupling between waveguided modes and different orientations of the transition dipole moment was investigated.

Acknowledgments

The work leading to these results has received funding from the IWT (Flemish Institute for Science and Technology). The authors acknowledge the Belgian Science Policy (project IAP 6/10-photonics@be). The work leading to these results has received funding from the European Community's Seventh Framework Programme under grant agreement no. FP7-224122 (OLED100.eu).

References

[1] Penninck, L., De Visschere, P., Beeckman, J., & Neyts, K. (2011). *Optics Express*, *19*, 18558–18576.

[2] Coles, H., & Morris, S. (2010). *Nature Photonics*, *4*, 676–685.

[3] Mulder, C. L., Reusswig, P. D., Velázquez, A. M., Kim, H., Rotschild, C., & Baldo, M. A. (2010). *Optics Express*, *18*, A79–A90.

[4] De Cort, W., Beeckman, J., James, R., Fernandez, F. A., Baets, R., & Neyts, K. (2009). *Optics Letters*, *34*, 2054–2056.

[5] Driesen, K., Moors, D., Beeckman, J., Neyts, K., Gorller-Walrand, C., & Binnemans, K. (2007). *Journal of Luminescence*, *127*, 611–615.

[6] Aldred, M. P., Contoret, A. E. A., Farrar, S. R., Kelly, S. M., Mathieson, D., O'Neill, M., Tsoi, W. C., & Vlachos, P. (2005). *Advanced Materials*, *17*, 1368–1372.

[7] Lukishova, S. G., Bissell, L. J., Menon, V. M., Valappil, N., Hahn, M. A., Evans, C. M., Zimmerman, B., Krauss, T. D., Stroud, C. R., & Boyd, R. (2009). *Journal of Modern Optics*, *56*, 167–174.

[8] O'Neill, M., & Kelly, S. M. (2003). *Advanced Materials*, *15*, 1135–1146.

[9] Lukosz, W. (1980). *Physical Review B*, *22*, 3030–3038.

[10] Neyts, K. (1998). *Journal of the Optical Society of America. A, Optics image science and Vision*, *15*, 962–971.

[11] Wasey, J. A. E., Safonov, A., Samuel, I. D. W., & Barnes, W. L. (2000). *Optics Communications*, *183*, 109–121.

[12] Bermel, P., Lidorikis, E., Fink, Y., & Joannopoulos, J. D. (2006). *Physical Review B*, *73*, 165125.

[13] Bienstman, P., Vandersteegen, P., & Baets, R. (2007). *Optical and Quantum Electronics*, *39*, 797–804.

[14] Lukosz, W. (1981). *Journal of the Optical Society of America*, *71*, 744–754.

[15] Clemmow, P. C. (1963). *Electrical Engineers, Proceedings of the Institution of*, *110*, 101–106.

[16] Bermel, P., Joannopoulos, J. D., Fink, Y., Lane, P. A., & Tapalian, C. (2004). *Physical Review B*, *69*, 035316.

[17] Ko, D. Y. K., & Sambles, J. R. (1988). *Journal of the Optical Society of America. A, Optics image science and Vision*, *5*, 1863–1866.

[18] Berreman, D. W. (1972). *Journal of the Optical Society of America*, *62*, 502–510.

[19] Beeckman, J., Neyts, K., & Haelterman, M. (2006). *Journal of Optics a-Pure and Applied Optics*, *8*, 214–220.